Development 138, 3885-3895 (2011) doi:10.1242/dev.065656


# Regulation of extra-embryonic endoderm stem cell differentiation by Nodal and Cripto signaling

**Marianna Kruithof-de Julio[1,2], Mariano J. Alvarez[2,3], Antonella Galli[1,2], Jianhua Chu[1,2], Sandy M. Price[4], Andrea Califano[2,3] and Michael M. Shen[1,2,*]**

## SUMMARY

The signaling pathway for Nodal, a ligand of the TGFβ superfamily, plays a central role in regulating the differentiation and/or maintenance of stem cell types that can be derived from the peri-implantation mouse embryo. Extra-embryonic endoderm stem (XEN) cells resemble the primitive endoderm of the blastocyst, which normally gives rise to the parietal and the visceral endoderm in vivo, but XEN cells do not contribute efficiently to the visceral endoderm in chimeric embryos. We have found that XEN cells treated with Nodal or Cripto (Tdgf1), an EGF-CFC co-receptor for Nodal, display upregulation of markers for visceral endoderm as well as anterior visceral endoderm (AVE), and can contribute to visceral endoderm and AVE in chimeric embryos. In culture, XEN cells do not express Cripto, but do express the related EGF-CFC co-receptor Cryptic (Cfc1), and require Cryptic for Nodal signaling. Notably, the response to Nodal is inhibited by the Alk4/Alk5/Alk7 inhibitor SB431542, but the response to Cripto is unaffected, suggesting that the activity of Cripto is at least partially independent of type I receptor kinase activity. Gene set enrichment analysis of genome-wide expression signatures generated from XEN cells under these treatment conditions confirmed the differing responses of Nodal- and Cripto-treated XEN cells to SB431542. Our findings define distinct pathways for Nodal and Cripto in the differentiation of visceral endoderm and AVE from XEN cells and provide new insights into the specification of these cell types in vivo.

**KEY WORDS: XEN cells, Visceral endoderm, AVE, Nodal, EGF-CFC proteins, Mouse**

## INTRODUCTION

During mammalian preimplantation development, an initial cell fate decision occurs during morula compaction, when outer cells become specified to form the trophectoderm, which will give rise to the trophoblast and extra-embryonic ectoderm, whereas inner cells will generate the pluripotent inner cell mass of the blastocyst (reviewed by Arnold and Robertson, 2009; Rossant and Tam, 2009; Zernicka-Goetz et al., 2009). A second cell fate restriction occurs prior to implantation, when the inner cell mass gives rise to the epiblast (primitive ectoderm) and the primitive endoderm. Following implantation, the primitive endoderm generates the visceral endoderm that surrounds the epiblast and extra-embryonic ectoderm, as well as the parietal endoderm that interacts with trophoblast cells.

Many studies have now demonstrated the crucial role of the visceral endoderm in epiblast patterning and differentiation. In particular, a central role in anterior-posterior (A-P) axis specification is played by the anterior visceral endoderm (AVE), a specialized population of cells within the visceral endoderm that overlies and patterns the adjacent epiblast at pregastrulation and early gastrulation stages (Arnold and Robertson, 2009; Rossant and Tam, 2009). In early postimplantation stages, at ~5.0 days post-coitum (dpc), the visceral endoderm overlying the epiblast (the embryonic visceral endoderm, EmVE) becomes morphologically and molecularly distinct from the visceral endoderm overlying the extra-embryonic ectoderm (the extra-embryonic visceral endoderm, ExVE) (Mesnard et al., 2006). Following the differentiation of EmVE, the distal visceral endoderm (DVE) forms in the most distal portion of the postimplantation egg cylinder at 5.0-5.25 dpc, and then translocates to the prospective anterior side through active directional cell migration by 6.0 dpc (Migeotte et al., 2010; Rivera-Perez et al., 2003; Srinivas et al., 2004; Stuckey et al., 2011; Takaoka et al., 2011; Thomas et al., 1998; Torres-Padilla et al., 2007; Trichas et al., 2011).

The proper differentiation of the EmVE as well as the formation and movement of the DVE require Nodal, a transforming growth factor beta (TGFβ) ligand that plays a central role in early vertebrate embryogenesis (Schier, 2009; Shen, 2007). Notably, the activity of Nodal requires epidermal growth factor-Cripto/FRL-1/Cryptic (EGF-CFC) co-receptors such as Cripto and Cryptic (Tdgf1 and Cfc1 – Mouse Genome Informatics) (Reissmann et al., 2001; Yan et al., 2002; Yeo and Whitman, 2001). In particular, membrane-bound Cripto appears to recruit Nodal to an activin receptor complex composed of a dimer of the type I serine-threonine receptor Alk4 (Acvr1b) and a dimeric type II activin receptor, either ActRII or ActRIIB (Acvr2a or Acvr2b – Mouse Genome Informatics). Following receptor activation, Smad2 and/or Smad3 are phosphorylated and accumulate together with Smad4 in the nucleus to mediate transcriptional responses (Yan et al., 2002; Yeo and Whitman, 2001). The activated Smad2-Smad4 complex interacts with nuclear transcription factors that include the FoxH1 (Fast2) winged-helix transcription factor (Chen et al., 1996; Chen et al., 1997). In the absence of EGF-CFC proteins, Nodal lacks signaling activity through activin receptors, in contrast to activin, which does not seem to require a co-receptor for its signaling activity (Gritsman

[1]Departments of Medicine, and Genetics and Development, Columbia University Medical Center, New York, NY 10032, USA. [2]Herbert Irving Comprehensive Cancer Center, Columbia University Medical Center, New York, NY 10032, USA. [3]Department of Biomedical Informatics and Center for Computational Biology and Bioinformatics, Columbia University Medical Center, New York, NY 10032, USA. [4]Center for Advanced Biotechnology and Medicine, University of Medicine and Dentistry of New Jersey – Robert Wood Johnson Medical School, Piscataway, NJ 08854, USA.

*Author for correspondence (mshen@columbia.edu)

**Accepted 30 June 2011**

et al., 1999; Kumar et al., 2001; Yan et al., 2002). Interestingly, soluble Cripto protein can also display signaling activity in cell culture and in vivo, indicating that EGF-CFC proteins can display trans-acting activities (Chu et al., 2005; Yan et al., 2002).

Numerous studies have shown that Nodal and its EGF-CFC co-receptors are required for multiple aspects of EmVE differentiation and formation of the DVE. In the absence of Nodal, the EmVE retains an extra-embryonic morphology and pattern of marker expression, indicating a role for Nodal in the differentiation of the EmVE (Mesnard et al., 2006). Moreover, Nodal signaling is essential for DVE specification, as no evidence of a DVE or a molecular or morphological A-P axis is apparent in *Nodal* null mutants or in *Cripto; Cryptic* double mutants (Brennan et al., 2001; Chu and Shen, 2010; Norris et al., 2002).

In principle, the analysis of primitive endoderm formation and its subsequent differentiation can be facilitated by the isolation of stem cell lines with primitive endoderm characteristics. Such XEN cell lines can be isolated from the mouse primitive endoderm and display many of the expected morphological and molecular properties of primitive endoderm cells (Artus et al., 2010; Brown et al., 2010; Kunath et al., 2005). Curiously, however, these XEN cells can only contribute efficiently to parietal endoderm in chimeras and only very rarely can contribute to visceral endoderm (Kunath et al., 2005).

We have investigated the possibility that Nodal signaling regulates the differentiation of visceral endoderm and AVE from XEN cells. We show that treatment of XEN cells with recombinant Nodal or Cripto proteins leads to visceral endoderm and AVE differentiation in culture and to their contribution to these tissues in chimeric embryos. Unexpectedly, the effects of Cripto treatment are distinct from those of Nodal as they are not inhibited by treatment with the Alk4/Alk5/Alk7 kinase inhibitor SB431542. In combination with bioinformatic analyses of global gene expression patterns, we conclude that Nodal and Cripto act through distinct signaling pathways to mediate visceral endoderm differentiation by XEN cells.

## MATERIALS AND METHODS

### XEN cell derivation and culture

Most of the experiments shown were performed using XEN cells from an enhanced yellow fluorescent protein (YFP)-expressing cell line (passage 12), which was generously provided by Janet Rossant (Hospital for Sick Children Research Institute, Toronto, Canada). We have also derived six additional wild-type XEN cell lines: three from GFP-expressing Tg(CAG-EGFP)B5Nagy/J mice (Hadjantonakis et al., 1998) and three from Swiss-Webster mice. All experiments with the XEN-YFP line, except for bioinformatic analyses, have been replicated using at least one of the newly derived wild-type cell lines. In addition, we derived one *Cryptic* homozygous mutant XEN cell line and three heterozygous lines from intercrosses of *Cryptic* heterozygous mutant mice (Yan et al., 1999).

XEN cells were derived and cultured as previously described (Kunath et al., 2005). *Cryptic* homozygous and heterozygous mutant XEN cells were derived in hanging drops in 30% XEN cell medium with 15% FCS/70% conditioned medium (CM) from mouse embryonic fibroblasts supplemented with 25 ng/ml FGF4 (R&D Systems) and 1 μg/ml heparin (Sigma). After 10 days of culture, the resulting cell aggregates were collected and cultured in four-well plates coated with 0.1% gelatin (Sigma). At day 20, cells were passaged and replated into standard XEN cell medium to establish lines.

Differentiation of XEN cells was performed by addition of recombinant Nodal (50 ng/ml) or Cripto (100 ng/ml) (R&D Systems) to XEN cell cultures for a total of 4 days. Alternatively, we used CM from Nodal- or Cripto-overexpressing HEK 293T cell lines, which were generated as described (Yan et al., 2002). In some experiments, the Alk4/Alk5/Alk7 kinase inhibitor SB435142 (1 μM, Sigma), or DMSO (Sigma) as a control, was also added.

XEN cells were transfected with Lipofectamine LTX (Invitrogen) according to the manufacturer's instructions. Luciferase assays for Nodal signaling activity were performed as previously described (Yan et al., 2002). Relative luciferase activities represent the average of the results of at least three independent experiments performed in duplicate.

### Quantitative real-time PCR analysis and western blotting

Total RNA was isolated from XEN cells using the RNeasy mini RNA isolation kit (Qiagen). First-strand cDNA was prepared by random priming of Superscript III reverse transcriptase (Invitrogen) and analyzed by RT-PCR or quantitative real-time PCR (see Table S1 in the supplementary material) using a LightCycler instrument (Roche) and analyzed using LinRegPCR software (Ramakers et al., 2003).

For western blot experiments, $2\times10^5$ XEN cells were seeded 1 day prior to treatment with recombinant Nodal (50 ng/ml), Cripto (100 ng/ml), SB435142 (1 μM) and/or DMSO for 1 hour. Western blotting was performed with phospho-Smad2 (Ser465/467; 3108, Cell Signaling; 1:1000), Smad2 (511300, Invitrogen; 1:200) and β-actin (sc-47778, Santa Cruz; 1:500) antibodies as described (Yan et al., 2002).

### Chimera analysis and immunofluorescence

Chimeras were generated by injection of XEN cells into 3.5-dpc blastocysts, or by morula aggregation with 2.5-dpc embryos from ICR mice (Nagy et al., 2003). For blastocyst injection, 10-15 XEN cells were injected per embryo, followed by transfer into the uterus of 2.5-dpc pseudopregnant Swiss-Webster females. The resulting embryos were dissected at 6.5 dpc and analyzed by direct imaging or by whole-mount immunofluorescence using a Leica TCS SP5 confocal microscope. Immunofluorescent staining of whole-mount embryos was performed as described (Kwon et al., 2008) using Cerl primary antibody (R&D Systems; 1:300) and Alexa 555 secondary antibody (Invitrogen; 1:250). Immunofluorescent staining of cells was performed using Cerl (R&D Systems) or Afp (R&D Systems) primary antibodies, both at 1:600, and Alexa 555 secondary antibody (Invitrogen; 1:250).

### Gene expression profiling and data analysis

For gene expression profiling, total RNA was isolated using the MagMAX-96 total RNA isolation kit (Ambion). Total RNA (200 ng) was reverse transcribed and biotin labeled by in vitro transcription using the Illumina TotalPrep RNA amplification kit (Ambion). Then 1.5 μg of the resulting cRNA was hybridized on mouse WG-6 v2 BeadArrays (Illumina). Hybridization data were obtained with an iScan BeadArray scanner (Illumina) and pre-processed by variance stabilization and robust spline normalization implemented in the lumi package under the R-System (Du et al., 2008). Expression data are available from the Gene Expression Omnibus database under GSE23675.

Prior to unsupervised cluster analysis, the expression data were normalized between slides to remove potential slide-dependent systematic bias. The signal of each probe $k$ in array $i$ of slide $j$, $y_{kji}$, was normalized by subtracting the difference between the intra- and inter-slide means:

$$\frac{1}{n}\sum_{i} y_{kji} - \frac{1}{N}\sum_{j}\sum_{i} y_{kji} \quad ,$$

where $n$ and $N$ are the number of arrays per slide and the total number of arrays, respectively. In this way, the normalized intra-slide mean of probe $k$ is equal to the inter-slide mean. Hierarchical cluster analysis was performed with a complete linkage agglomerative algorithm (hclust function of R-System v2.8.0) using $1–r$, where $r$ is the Pearson's correlation coefficient, as distance metric. Principal components analysis (PCA) was performed with a singular value decomposition (SVD) algorithm (prcomp function of R-System v2.8.0).

For differential expression analysis, we did not apply any inter-slide normalization. We modeled the potential systematic bias by including a random factor for the experimental batch in a lineal model $y_k=\mu_k+\alpha_k+\beta_k+\varepsilon_k$, where $\alpha$ is the fixed treatment effect and $\beta$ is the random experimental batch effect. We fitted this model to the data and estimated the treatment $P$-value using the limma package implemented in R-System (Smyth, 2004). Redundant probes were eliminated by keeping the one showing the

highest dynamic range (coefficient of variation) among samples. False discovery rate (FDR) was estimated as described (Benjamini and Hochberg, 1995). Enrichment of Gene Ontology Biological Process (GO-BP) gene sets on Nodal and Cripto gene expression signatures were assessed by gene set enrichment analysis [GSEA (Subramanian et al., 2005)].

Statistical significance for the overlap between signatures was computed by Fisher's exact test and by a modified version of GSEA [two-tails GSEA (Lim et al., 2009)]. Briefly, we divided the query gene set into two subsets: a positive subset containing the upregulated part of the query signature, and a negative subset encompassing the downregulated part of the query signature. The target signature was then sorted from the most upregulated to the most downregulated gene (signature A) and the rank positions for the positive query subset were computed. The rank positions for the negative subset were computed from the target signature, but this time sorted from the most downregulated to the most upregulated gene (signature B). The enrichment score (ES) was computed as described (Subramanian et al., 2005), using the computed rank positions for the positive and negative subsets, but taking the score values only from signature A. The normalized enrichment score (NES) and nominal *P*-values were estimated by uniformly permuting the query signature ranks 10,000 times. Genes in common between two signatures were obtained from the union of the leading-edge gene sets (Subramanian et al., 2005).

## RESULTS

### Nodal pathway activation promotes visceral endoderm differentiation by XEN cells

To investigate the potential role of Nodal pathway activity in primitive endoderm, we examined the ability of XEN cells to differentiate into visceral endoderm following Nodal or Cripto treatment, using a YFP-expressing mouse XEN cell line. In our studies, we have found that treatment of these XEN-YFP cells with recombinant Nodal or Cripto protein over 4 days of culture leads to upregulation of the visceral endoderm marker alpha fetoprotein (Afp) (Fig. 1A-F,J). We obtained similar results using conditioned medium produced from *Nodal*- or *Cripto*-overexpressing HEK 293T cell lines (Yan et al., 2002) and have confirmed these observations using six different wild-type XEN cell lines produced in our laboratory (see Fig. S1A in the supplementary material; data not shown). Similarly, a significant percentage of treated XEN cells display upregulation of the AVE marker Cerberus-like (Cerl; Cer1 – Mouse Genome informatics) (Fig. 1G-J; see Fig. S1A in the supplementary material), as 17.8±1.8% of Nodal-treated and 17.7±1.1% of Cripto-treated cells displayed Cerl immunostaining. We also observed upregulation of E-cadherin, which is expressed by visceral endoderm and not parietal endoderm (see Fig. S2 in the supplementary material). By contrast, no effects were observed on the expression of the visceral endoderm marker *Hnf4a* or the primitive endoderm markers *Sox7*, *Gata4* and *Gata6*; as expected, the epiblast marker *Oct4* (*Pou5f1* – Mouse Genome informatics) and the trophectoderm marker *Cdx2* were not expressed (Fig. 1J; see Fig. S1 in the supplementary material). Quantitative real-time PCR analyses confirmed significant upregulation for both *Afp* and *Cerl* following treatment with Nodal or Cripto, whereas little or no effect was observed on the expression of *Gata6* and *Hnf4a* (Fig. 1K). Despite these alterations in gene expression, we did not observe significant changes in the morphology of the Nodal- or Cripto-treated XEN cells after 4 days of culture (Fig. 1A-C).

### Requirement for *Cryptic* in mediating Nodal signaling in XEN cells

Given the response of XEN cells to Nodal and Cripto treatment, we next examined the expression of genes encoding components of the Nodal signaling pathway. Previous studies have shown that

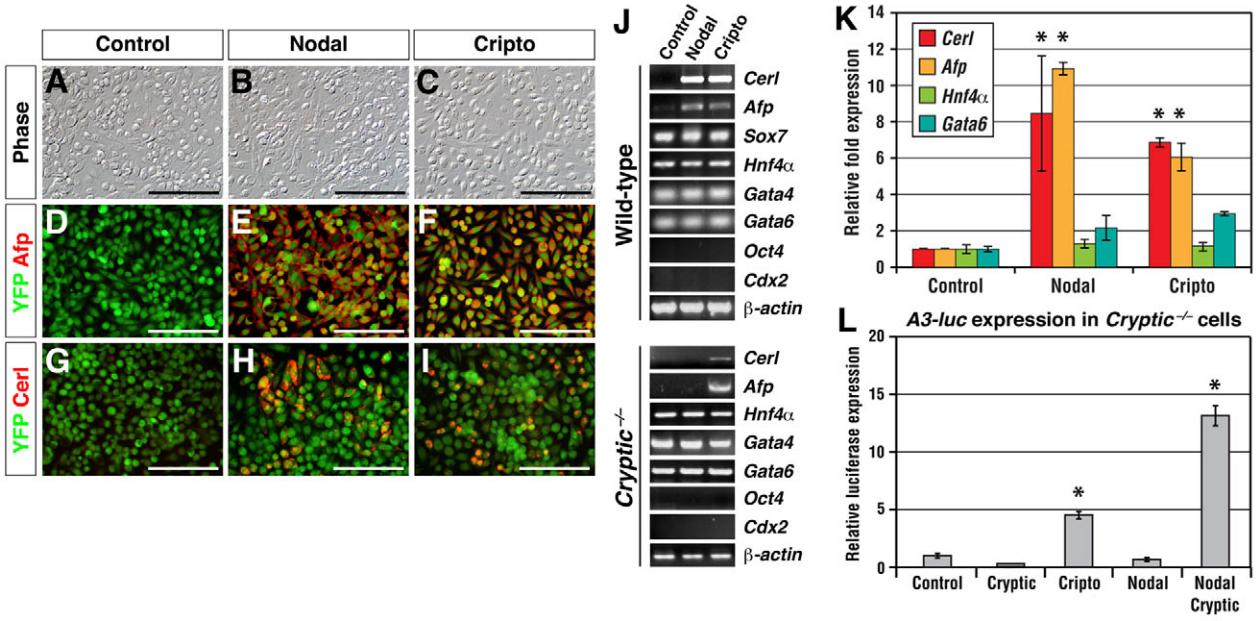


**Fig. 1. Nodal and Cripto promote visceral endoderm differentiation of XEN cells in culture.** (**A-C**) Mouse extra-embryonic endoderm stem (XEN) cells show no significant alterations in cell morphology after 4 days of Nodal or Cripto treatment. (**D-I**) Treatment of YFP-expressing XEN cells with recombinant Nodal or Cripto for 4 days results in upregulation of the visceral endoderm markers Afp (D-F) and Cerl (G-I). (**J**) RT-PCR analysis of wild-type and *Cryptic*$^{-/-}$ XEN cells using the indicated markers and β-actin as a control. (**K**) Quantitative real-time PCR shows no significant variation in the expression of *Hnf4a* and *Gata6* after Nodal or Cripto treatment, whereas expression of both *Afp* and *Cerl* is significantly increased. (**L**) Luciferase assay for Nodal signaling activity in *Cryptic*$^{-/-}$ XEN cells by transient transfection of the indicated expression vectors together with the *A3-luc* reporter. No activity is detected in response to Nodal unless the Cryptic co-receptor is co-expressed. *, $P<0.05$, relative to control. Error bars indicate s.d. Scale bars: 50 μm.

this pathway can be activated by TGFβ ligands in addition to Nodal, including mammalian growth differentiation factor 1 (Gdf1) and Gdf3 (Andersson et al., 2007; Andersson et al., 2008; Andersson et al., 2006; Chen et al., 2006; Cheng et al., 2003). Although Gdf1 may act as a co-ligand for Nodal (Tanaka et al., 2007), Gdf3 appears to have intrinsic signaling activity, utilizing either the Alk4 or Alk7 (Acvr1c) type I receptors (Andersson et al., 2007; Andersson et al., 2008; Andersson et al., 2006; Chen et al., 2006; Cheng et al., 2003). We found that *Alk4*, *Alk5* (*Tgfbr1*), *ActRIIB* and *Foxh1* were expressed by XEN cells in all treatment conditions, without significant changes in their levels in response to Nodal or Cripto (see Fig. S1B in the supplementary material). By contrast, expression of *Nodal*, *Gdf1*, *Gdf3* and *Alk7* was not observed (see Fig. S1B in the supplementary material). Notably, XEN cells do not express the EGF-CFC co-receptor *Cripto*, but do express the related co-receptor *Cryptic* (see Fig. S1B in the supplementary material).

To determine whether the EGF-CFC co-receptor Cryptic mediates the response to Nodal in XEN cells, we derived a new XEN cell line, XEN-TIC1, which is homozygous for a *Cryptic* null mutation as derived from intercrosses of *Cryptic* heterozygous mutant mice. We examined the activity of Nodal, Cripto and Cryptic in this *Cryptic* mutant XEN cell line using a modification of a luciferase reporter assay that we previously developed to investigate Nodal signaling in HEK 293T cells (Yan et al., 2002). This assay for Nodal relies upon the co-expression of an EGF-CFC co-receptor and FoxH1 in transfected cells and the measurement of the activity of luciferase expressed by the activin/Nodal-responsive reporter *A3-luc*. Since XEN cells already express *Foxh1*, we measured luciferase activity following transfection of Nodal, Cripto and/or Cryptic expression vectors into the XEN-TIC1 cells. As expected, we found that expression of Nodal or Cryptic alone did not result in luciferase activity in the XEN-TIC1 cells, whereas Cripto alone stimulated luciferase activity 4.5-fold relative to the control (Fig. 1L). However, luciferase activity was strongly stimulated by co-transfection of Nodal with Cryptic, indicating that Nodal signaling remains EGF-CFC-dependent in XEN-TIC1 cells (Fig. 1L). These results were confirmed by analyses of AVE and visceral endoderm marker expression in the XEN-TIC1 cells (Fig. 1J). Thus, these findings indicate that the response to Nodal signaling in XEN cells is Cryptic dependent.

## Differentiation of visceral endoderm and AVE in chimeric embryos

To determine the behavior of XEN cells in vivo, we generated chimeric embryos by blastocyst injection of XEN cells (Table 1), using either the original XEN-YFP line or one of our newly derived XEN lines that expresses GFP. In control chimeras generated by injection of untreated XEN cells, we observed contribution exclusively to parietal endoderm when analyzed at 6.5 dpc ($n$=18) (Fig. 2A), as reported previously (Kunath et al., 2005). However, consistent with our finding in cell culture, chimeras produced with either Nodal- or Cripto-treated XEN cells displayed a significant contribution to visceral endoderm ($n$=10 chimeras for Nodal treatment, $n$=16 for Cripto), with occasional contribution to parietal endoderm (Fig. 2B,C,G; see Fig. S3A,B in the supplementary material). We did not observe any obvious regional differences in the contribution of Nodal-treated or Cripto-treated XEN cells to the EmVE or ExVE (Fig. 2B,C,G; see Fig. S3A,B in the supplementary material).

We also generated chimeras by morula aggregation, obtaining integration of XEN cells ($n$=14/20) and Nodal-treated XEN cells into the blastocyst inner cell mass at 3.5 dpc ($n$=6/12 blastocysts) (Fig. 2D; data not shown). Similar to the chimeras generated by blastocyst injection, we observed contribution of Nodal-treated XEN cells to the visceral endoderm at 6.5 dpc ($n$=3) in morula aggregation chimeras (Fig. 2E,F; see Movie 1 in the supplementary material).

Finally, to determine whether treated XEN cells contribute to AVE in vivo, we examined the colocalization of GFP expressed by the XEN cells with Cerl, which marks the AVE at 6.5 dpc. Nodal-treated and Cripto-treated XEN cells injected into blastocysts resulted in chimeras containing cells that co-expressed Cerl and GFP, indicating the contribution of XEN cells to the AVE (Fig. 2G-J; see Fig. S3C-F in the supplementary material).

## Gene expression changes during XEN cell differentiation

To investigate the transcriptional response to Nodal and Cripto treatment, we performed genome-wide gene expression profiling of XEN cells at 4 days after Nodal or Cripto treatment. Four biological replicates for each condition were hybridized on mouse WG-6 v2 Illumina BeadArrays. From the 20,311 profiled genes, 4693 and 4704 were differentially expressed after Nodal and Cripto treatments, respectively (FDR<0.01) (Table 2; see Tables S2 and S3 in the supplementary material). To examine the transcriptional response to these treatments, we used principal components analysis (PCA), a method that projects data variability onto a reduced number of orthogonal axes, such that the first axis captures the greatest degree of variance, and subsequent axes correspond to successively decreasing variance. Notably, this approach demonstrated a similar transcriptional response to both Nodal and Cripto treatments, as shown by the first principal component (PC-1), which captures 75.1% of the data variability (Fig. 3A). This conclusion is also supported by unsupervised hierarchical cluster analysis (see Fig. S4 in the supplementary material), statistical analyses (see Table S5 in the supplementary material), and heatmap analysis of the expression of selected markers of primitive, visceral and definitive endoderm, as well as TGFβ pathway components (see Fig. S5 in the supplementary material). Furthermore, there is a strong overlap between the Nodal gene expression signature and the Cripto signature (odds ratio=52.7, $P<10^{-16}$ by Fisher's exact test) (Fig. 3B).

**Table 1. Summary of XEN cell chimera analysis**

| | Control | Nodal | Cripto | SB431542 | Nodal+ SB431542 | Cripto+ SB43152 |
|---|---|---|---|---|---|---|
| Embryos transferred | 313 | 179 | 286 | 16 | 59 | 79 |
| Embryos recovered | 74 (23.6%*) | 35 (19.6%*) | 69 (24.1%*) | 2 (12.5%*) | 26 (44.1%*) | 20 (25.3%*) |
| Chimeras | 18 (24.3%†; 5.8%*) | 10 (28.6%†; 5.6%*) | 16 (23.2%†; 5.6%*) | 0 | 7 (26.9%†; 11.9%*) | 7 (35.0%†; 8.9%*) |

Embryo chimeras were generated by blastocyst injection of XEN cells and analyzed at 6.5 dpc.
*Percentage of transferred; †percentage of recovered.

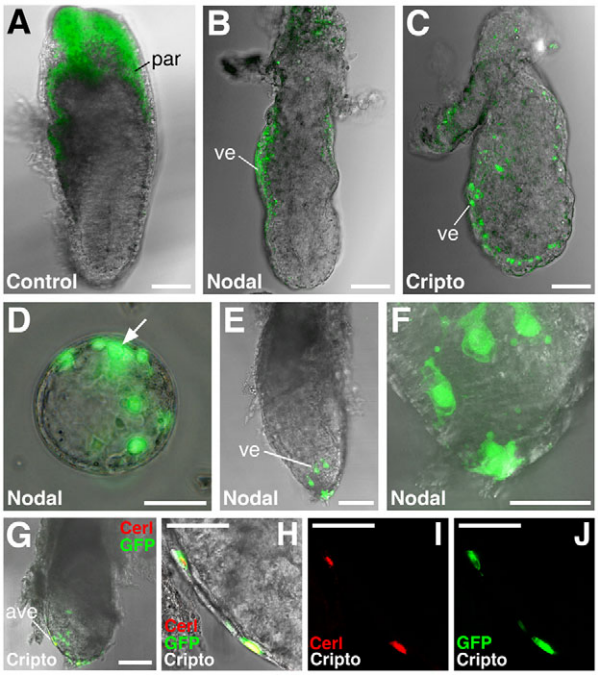


**Fig. 2. Contribution of treated XEN cells to visceral endoderm and AVE in chimeric embryos.** (**A**) Chimeras generated from control YFP-expressing XEN cells only show contribution to parietal endoderm at 6.5 dpc. (**B**,**C**) Chimeras generated by blastocyst injection of Nodal- or Cripto-treated XEN cells show contribution to visceral endoderm at 6.5 dpc. (**D**) Contribution of Nodal-treated XEN cells (arrow) to the blastocyst inner cell mass at 3.5 dpc following morula aggregation. (**E**,**F**) Chimera generated by morula aggregation using Nodal-treated XEN cells shows contribution to visceral endoderm at 6.5 dpc. (**G-J**) Confocal immunofluorescence imaging of a chimeric 6.5 dpc mouse embryo generated by blastocyst injection of Cripto-treated XEN cells, shown at low (G) and high (H-J) magnification as an overlay (H) and as individual channels (I,J). Co-expression of YFP with the anterior visceral endoderm (AVE) marker Cer1 (red) is observed; note that other Cer1-expressing cells are out of the plane of the optical section. ve, visceral endoderm; par, parietal endoderm. Scale bars: 100 μm in A-C,E,G; 50 μm in D,F,H-J.

We further inspected the similarity of the Nodal and Cripto gene expression signatures using gene set enrichment analysis (GSEA), which is an unsupervised methodology that is specifically designed for computing the overlap between gene expression signatures (Subramanian et al., 2005). GSEA is a useful analytical method because genes in a signature (e.g. those regulated by Cripto) might not have large fold changes, but do display correlated responses when a different treatment is applied (e.g. treatment with Nodal), indicating coordinated regulation. Indeed, GSEA is the most effective approach to test whether two processes produce similar effects in terms of differentially expressed genes (Subramanian et al., 2005). Using an enhanced version of this algorithm, termed two-tails GSEA, which takes into account the 'direction' of the gene expression change (Lim et al., 2009), we found a strong enrichment of the Nodal signature on the Cripto gene expression profile (Fig. 3C) and vice versa (Fig. 3D). Consistent with these findings, we found only 64 genes that responded in opposite directions to Nodal and Cripto treatments, with just three genes displaying more than 2-fold change in gene expression in either signature (see Table S4 in the supplementary material). These reciprocal enrichment data strongly support the similar outcomes following Nodal or Cripto treatment of XEN cells and are highly consistent with our cell culture and chimera data in vivo.

To obtain insights into the biological processes modulated by Nodal and Cripto treatment, we determined the Gene Ontology-Biological Process (GO-BP) gene sets that were significantly enriched in the Nodal and Cripto gene expression signatures (see Table S6 in the supplementary material). We found that 54 GO-BP categories were enriched in the Nodal signature and 46 in the Cripto signature, with 31 categories enriched in both signatures.

## Cripto activity on XEN cells is Nodal independent

Our gene expression analyses revealed that XEN cells do not express detectable levels of *Nodal* or of *Gdf1* and *Gdf3*, which encode potential Nodal-like signaling factors or Nodal co-ligands (see Fig. S1B in the supplementary material). Consequently, it is unclear how Cripto treatment could affect the differentiation of XEN cells, as the known EGF-CFC-dependent ligands are not expressed. One possibility is that the addition of Cripto could mediate the activity of another, as yet unidentified, TGFβ ligand, which could then signal through the canonical Nodal/activin/TGFβ pathway. To investigate this possibility, we utilized the small molecule inhibitor SB431542, which blocks the kinase activity of the type I receptors Alk4, Alk5 and Alk7 (Inman et al., 2002), and thereby inhibits Nodal pathway signaling. As expected, we found that treatment with 1 μM SB431542 inhibits visceral endoderm differentiation stimulated by recombinant Nodal, as assessed by expression of *Afp*, *Cerl* and E-cadherin, but has little effect by itself (Fig. 4A,B,D,E,G,H,J,K; see Fig. S2 in the supplementary material). No significant effects on expression of *Sox7*, *Hnf4a*, *Gata4* or *Gata6* were observed in response to SB431542, whereas *Oct4* and *Cdx2* were not expressed (Fig. 4J,K). Furthermore, the expression levels of *Foxh1*, *Cryptic* and *Alk4* were unaffected in all treatment conditions, whereas *Nodal*, *Gdf1* and *Cripto* were not expressed (see Fig. S1B in the supplementary material).

Unexpectedly, however, SB431542 treatment did not inhibit visceral endoderm differentiation induced by Cripto (Fig. 4C,F,I; see Fig. S1 in the supplementary material). Analyses of marker gene expression confirmed that SB431542 blocks the effects of Nodal treatment, but not those of Cripto (Fig. 4J,K); in particular, 14.4±1.4% of cells treated with Cripto and SB431542 displayed Cerl immunostaining. Furthermore, in chimera analyses, we found that XEN cells treated with both Nodal and SB431542 only contribute to the parietal endoderm ($n$=7) (Fig. 4L,M), as expected for inhibition of Nodal pathway activity. By contrast, XEN cells treated with both Cripto and SB431542 maintained their ability to contribute to visceral endoderm and AVE ($n$=7) (Fig. 4N,O; see Fig. S3G-L in the supplementary material).

Next, we performed expression profiling of Nodal- and Cripto-treated XEN cells in the presence of SB431542, and compared the resulting expression signatures with those generated in the absence of SB431542. PCA revealed that SB431542 significantly impaired the Nodal gene expression signature (Fig. 5A, Table 2), consistent with the unsupervised hierarchical clustering analysis (see Fig. S4 in the supplementary material). In particular, two-tails GSEA showed no significant enrichment of the Nodal signature on the Nodal+SB431542 gene expression profile (Fig. 5B). Conversely, SB431542 did not substantially affect the Cripto gene expression signature, as shown by the unsupervised analysis (Fig. 5A; see Fig. S4 in the supplementary material). This conclusion is further supported by the significant overlap between the Cripto and Cripto+SB431542 gene expression signatures (odds ratio=78.7,

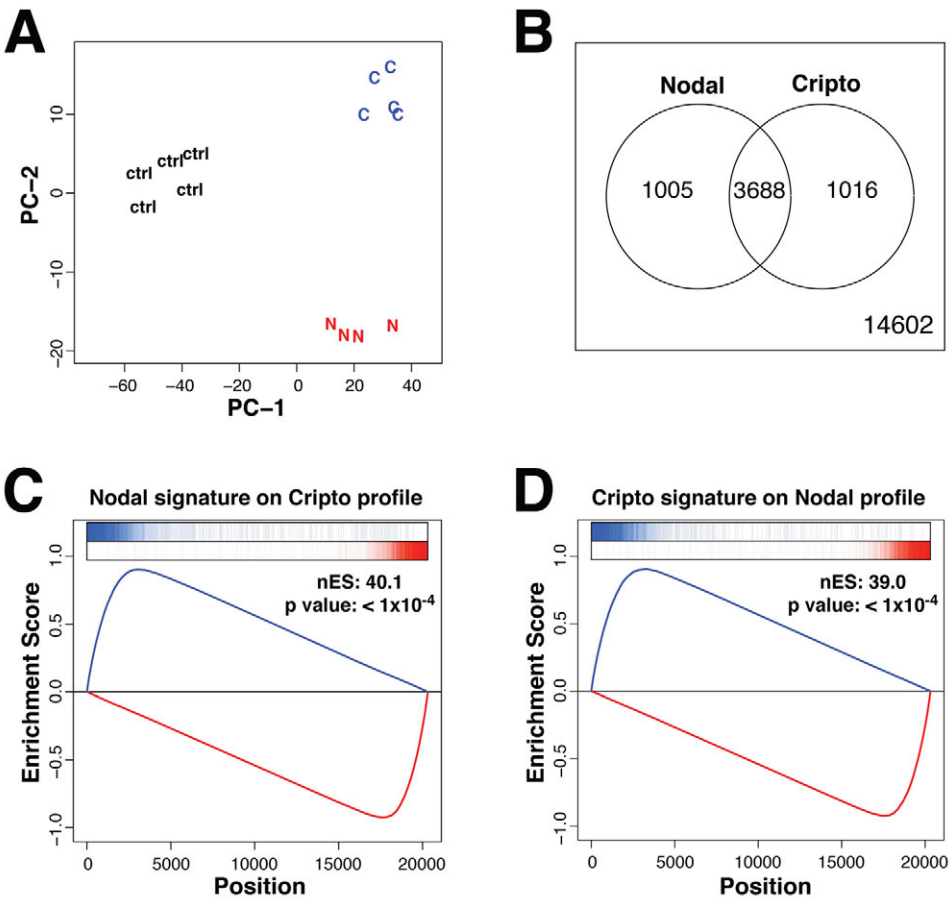


**Fig. 3. Effect of Cripto and Nodal on XEN cell gene expression profiles.** (**A**) Scatter plot of the two main components from a principal components analysis (PCA) based on all 45,281 probes, capturing 75.1% (principal component 1, PC-1) and 8.84% (PC-2) of the data variability. Labels indicate the positions for control XEN cells (ctrl), Nodal-treated (N) and Cripto-treated (C) XEN cells. Note that the Nodal and Cripto responses overlap with respect to PC-1. (**B**) Venn diagram showing the overlap between Nodal and Cripto gene expression signatures (odds ratio=52.7, $P<10^{-15}$). (**C**) Two-tails gene set enrichment analysis (GSEA) of the Nodal treatment signature on the Cripto gene expression profile. Shown on the *x*-axis is the rank order of genes from the most downregulated (position 1) to the most upregulated (position 20,311) after Cripto treatment. The two barcode-like plots at the top of the graph indicate the positions of the upregulated (red) and downregulated (blue) genes in response to Nodal treatment on the rank-sorted Cripto gene expression profile. The *y*-axis corresponds to the running enrichment score (ES) generated by the cumulative tally, moving left to right, of when a Nodal signature gene is present in the Cripto expression profile (which moves the curve up) or when a Nodal signature gene is absent (which moves the curve down). The total height of the curve indicates the extent of enrichment, with the normalized enrichment score (nES) corresponding to the deviation from a null model (normal distribution with variance of 1). The blue curve represents the genes that are downregulated in response to Nodal, whereas the red curve corresponds to upregulated genes. A positive enrichment score for the blue curve indicates an enrichment of the Nodal downregulated genes on the left tail of the Cripto gene expression profile, whereas a negative enrichment score for the red curve indicates enrichment of the Nodal upregulated genes on the right tail of the Cripto gene expression profile. The genes located to the left of the maximum of the blue curve and those located to the right of the absolute maximum of the red curve constitute the leading-edge gene sets. (**D**) Two-tails GSEA of the Cripto treatment signature on the Nodal gene expression profile.

$P<10^{-16}$ by Fisher's exact test) (Fig. 5C), by the strong enrichment of the Cripto gene expression signature on the Cripto+SB431542 gene expression profile (Fig. 5D), by the unsupervised hierarchical cluster analysis (see Fig. S4 in the supplementary material) and by the heatmap analysis of selected gene expression (see Fig. S5 in the supplementary material). Consistent with this conclusion, we found only 37 genes that responded in opposite directions to Cripto versus Cripto+SB431542, with just three genes displaying a greater than 2-fold enrichment in either signature (see Table S7 in the supplementary material). In combination with the cell culture and chimera analyses, these results indicate that the effects of Cripto on XEN cells are largely independent of Alk4/Alk5/Alk7 receptor kinase activity.

## Cripto signaling upregulates Smad2 phosphorylation in XEN cells

Based on the similarity of the functional response to Nodal and Cripto in XEN cells, we investigated whether they shared a similar downstream response through the phosphorylation of Smad2. Treatment of XEN cells with Nodal or Cripto resulted in increased levels of C-terminal phosphorylated Smad2 (pSmad2, Ser465/467), as detected by immunofluorescence and western blotting (Fig. 6); moreover, we observed no alterations in the overall levels of Smad2 (Fig. 6G). These results indicate that both Nodal and Cripto treatments activate the canonical Nodal/activin/TGFβ pathway through phosphorylation of Smad2. However, SB431542 blocked Nodal-dependent as well as Cripto-dependent Smad2

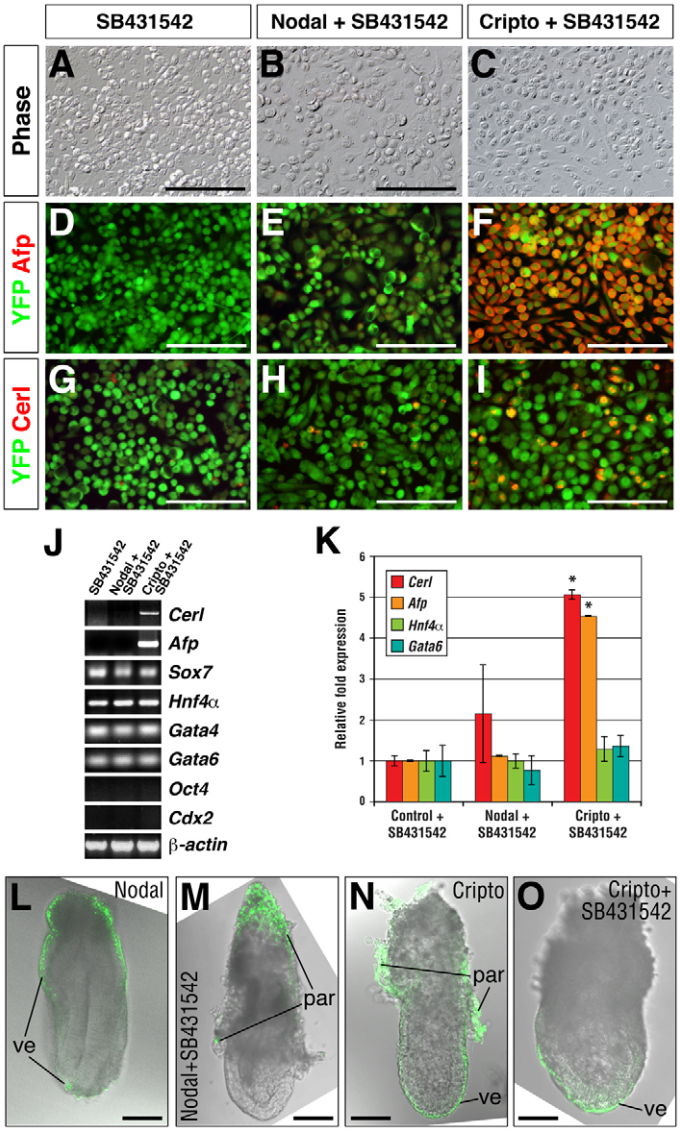


**Fig. 4. Activity of Cripto on XEN cells is not inhibited by SB431542.** (**A-C**) SB431542 treatment of mouse XEN cells for 4 days does not result in detectable alterations in cell morphology. (**D-I**) Treatment of XEN cells for 4 days with recombinant Nodal in the presence of SB431542 inhibits upregulation of the visceral endoderm markers Afp (E) and Cer1 (H), whereas SB431542 does not inhibit upregulation of expression of Afp (F) and Cer1 (I) in response to Cripto treatment. Note that the experiment shown in A-I was performed in parallel with the experiment shown in Fig. 1A-I. (**J**) RT-PCR analysis shows that expression of *Afp* and *Cer1* was only detectable after Cripto+SB431542 treatment, but not after Nodal+SB431542 treatment; no effects of SB431542 were observed on the expression of the other markers examined. (**K**) Quantitative real-time PCR confirms that expression of *Cerl* and *Afp* was significantly increased in response to Cripto+SB431542 treatment, but not after Nodal+SB431542 treatment. *, *P*-value<0.05, relative to control. Error bars indicate s.d. (**L**,**M**) Chimeras generated by blastocyst injection of Nodal-treated cells show contribution to visceral endoderm (L), but Nodal+SB431542-treated cells only contribute to parietal endoderm (M). (**N**,**O**) Both Cripto-treated (N) and Cripto+SB431542-treated (O) XEN cells contribute to visceral endoderm; note that some parietal endoderm contribution is found in the embryo in N. ve, visceral endoderm; par, parietal endoderm. Scale bars: 50 μm in A-I; 100 μm in L-O.

phosphorylation, indicating that phosphorylation of Smad2 relies upon Alk4/Alk5/Alk7 kinase activity in XEN cells. These results indicate that Cripto can elicit Smad2 phosphorylation in an Alk4/Alk5/Alk7-dependent manner, similar to Nodal. By contrast, XEN cell differentiation into visceral endoderm and AVE in response to Cripto is at least partially independent of Alk4/Alk5/Alk7 kinase activity and Smad2 phosphorylation.

## DISCUSSION

Our findings reveal that Nodal signaling can alter the differentiation potential of XEN cells and provide new insights into the molecular regulation of Nodal signaling as well as the formation of visceral endoderm in vivo. We have shown that treatment of XEN cells with either Nodal or Cripto protein promotes their differentiation into visceral endoderm as well as AVE in culture and in chimeric embryos. Unexpectedly, our data also show that the activities of Nodal and Cripto are distinct, as the ability of Cripto to promote visceral endoderm and AVE differentiation is not blocked by SB431542. Furthermore, this activity of Cripto is at least partially independent of Smad2 phosphorylation because Smad2 phosphorylation in response to Cripto is inhibited by SB431542. Therefore, our findings raise the possibility that Cripto can signal, at least in part, through a downstream pathway in XEN cells that is independent of Alk4 kinase activity and Smad2 phosphorylation. Such a non-canonical signaling pathway might be significant for the molecular regulation of visceral endoderm and DVE formation in vivo.

### Potential mechanisms for Cripto signaling activity

Our results suggest a model in which Nodal and Cripto act cooperatively through distinct and possibly synergistic signaling pathways to regulate XEN cell differentiation into visceral endoderm and AVE. The addition of Nodal stimulates canonical signaling through Alk4 and Smad2/Smad3 to promote visceral endoderm and AVE differentiation, and this activity is dependent upon the EGF-CFC protein Cryptic (Fig. 7A). In the absence of Nodal, we propose that Cripto can either signal through type I receptors in a kinase-independent manner (which would not be inhibited by SB431542), or through an as yet unidentified novel receptor in XEN cells (Fig. 7B). Endogenous Cryptic activity would presumably be unable to activate either pathway in the absence of Nodal or Cripto, either because the levels of Cryptic are insufficient or because it is functionally dissimilar to Cripto.

This model contrasts with previous studies that have linked Cripto activity to the function of Nodal pathway ligands. Cripto is produced as a glycosylphosphatidylinositol (GPI)-linked protein, and can be readily detected in the culture medium of mammalian cells transfected with full-length Cripto expression constructs (Minchiotti et al., 2000; Yan et al., 2002). Soluble Cripto protein from culture medium, as well as commercially available recombinant protein, can stimulate Nodal pathway activity in a luciferase reporter assay in HEK 293T cells, where pathway activity requires Nodal ligand and can be inhibited by Lefty proteins (Chen and Shen, 2004; Yan et al., 2002). Furthermore, soluble Cripto can induce prechordal mesoderm differentiation from explants of chick notochord, and this activity is Alk4/Alk5/Alk7 dependent as it can be blocked by SB431542 (Chu et al., 2005). Although the mechanism by which soluble Cripto is produced in cell culture is unknown, a similar mechanism is likely to occur in vivo. Indeed, previous chimera analyses have demonstrated the non-cell-autonomy of Cripto function in the mesendoderm (Chu et al., 2005). Similarly, the non-overlapping

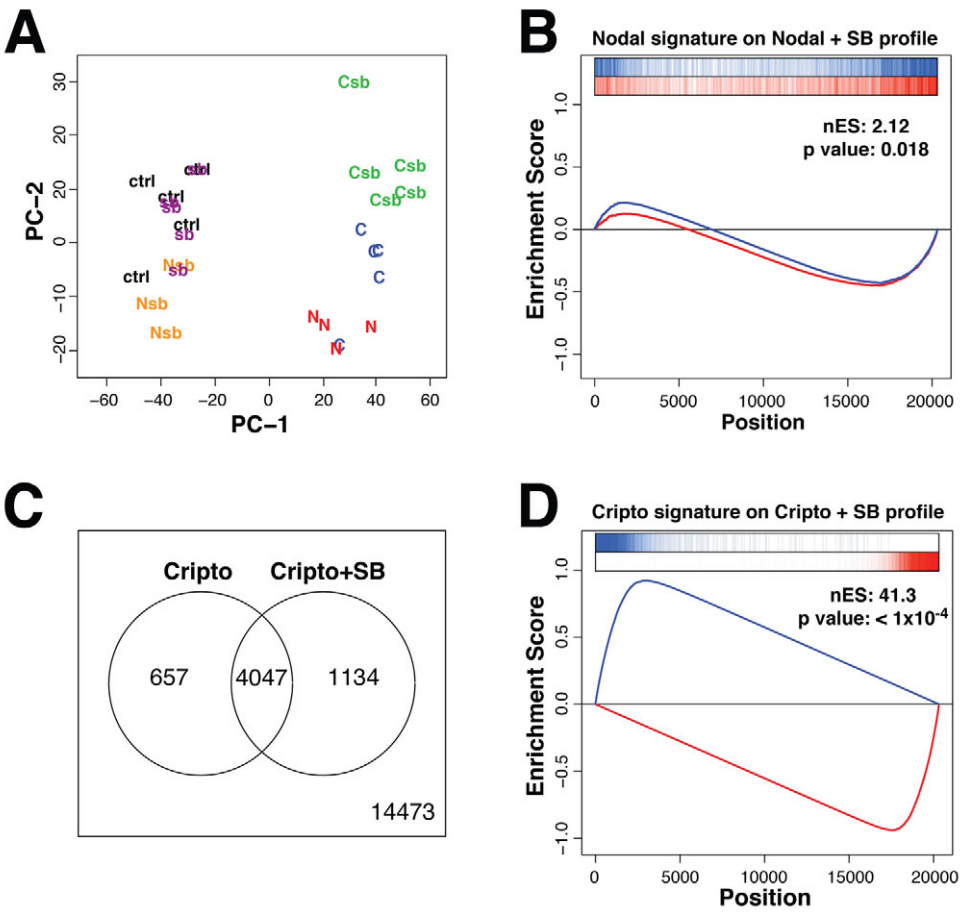


**Fig. 5. SB431542 blocks the Nodal but not Cripto gene expression signature.** (**A**) Scatter plot of the two main components from a PCA based on all 45,281 probes, capturing 73.6% (PC-1) and 8.22% (PC-2) of the data variability. Labels indicate the positions for control XEN cells (ctrl), Nodal-treated (N), Cripto-treated (C), SB431542-treated (sb), Nodal+SB431542-treated (Nsb) and Cripto+SB431542-treated (Csb) XEN cells. (**B**) Two-tails GSEA of the Nodal signature on the Nodal+SB431542 gene expression profile. The lack of enrichment for the Nodal signature is evident from the low normalized enrichment score and from the distribution of the Nodal upregulated and downregulated genes on the Nodal+SB431542 gene expression profile in the barcode-like plots at the top of the graph. (**C**) Venn diagram showing the overlap between the Cripto and Cripto+SB431542 gene expression signatures (odds ratio=78.7, $P<10^{-15}$). (**D**) Two-tails GSEA of the Cripto-induced visceral endoderm signature on the Cripto+SB431542 gene expression profile.

expression patterns of *Cripto* and *Cryptic* imply non-cell-autonomy in the visceral endoderm (Chu and Shen, 2010), supporting the conclusion that Cripto expressed in the epiblast can behave as a trans-acting factor in vivo to promote DVE formation.

Notably, there are several published reports of Nodal pathway-independent effects of Cripto in mammalian cell culture. Thus, Cripto can act as a non-competitive antagonist for activin (Adkins et al., 2003; Gray et al., 2003; Kelber et al., 2008), as well as an inhibitor for TGFβ (Gray et al., 2006; Shani et al., 2008). In other cases, Cripto has effects that appear to be independent of TGFβ pathway components, as it can signal independently of Alk4 through c-Src, resulting in downstream activation of the Ras/Raf/MAP kinase and phosphatidylinositol 3′-kinase (PI3K)-Akt pathways (Bianco et al., 2002; Bianco et al., 2003; Ebert et al., 1999). Activation of c-Src may be mediated by binding of Cripto to glypican-1, which is a GPI-linked heparan sulfate proteoglycan (Bianco et al., 2003). Furthermore, Cripto may also modulate another developmental signaling pathway, as a recent study has shown that human CRIPTO can potentiate Notch signaling by promoting enhanced proteolytic cleavage and maturation of Notch receptors (Watanabe et al., 2009). At present, it is conceivable that Cripto might signal in XEN cells through one of these previously described non-canonical pathways, which then converges on Nodal targets downstream of Smad2, or might instead modulate a novel non-canonical signaling pathway. However, the mechanisms by which Nodal and Cripto signaling lead to functional convergence with downstream components of the canonical Nodal signaling pathway remain to be investigated.

**Table 2. Differential gene expression in treated XEN cells**

| Treatment | FDR<0.05 | FDR<0.01 |
|---|---|---|
| Nodal | 5977 | 4693 |
| Cripto | 6032 | 4704 |
| SB431542 | 0 | 0 |
| Nodal+SB431542 | 4 | 1 |
| Cripto+SB431542 | 6540 | 5181 |

The number of differentially expressed genes relative to control untreated XEN cells is shown for each treatment condition.
FDR, false discovery rate.

## XEN cells can recapitulate the fates of primitive endoderm

Our findings on the properties of XEN cells in culture and chimeric embryos raise the possibility that Nodal and EGF-CFC proteins play a central role during the early steps of visceral endoderm specification and/or differentiation in vivo. This interpretation is consistent with previous analyses of the EmVE defects in *Nodal* mutants and *Cripto; Cryptic* double mutants (Chu and Shen, 2010; Mesnard et al., 2006). In addition, Nodal signaling stimulates visceral endoderm formation during human ES cell differentiation in culture (Vallier et al., 2005). Furthermore, our results are consistent with the view that Nodal and/or Cripto signal from the epiblast to the visceral endoderm to promote DVE formation. Although a central role for Nodal has been supported by several studies (Brennan et al., 2001; Chu and Shen, 2010; Norris et al., 2002), direct evidence for the ability of Nodal to induce DVE has been previously lacking.

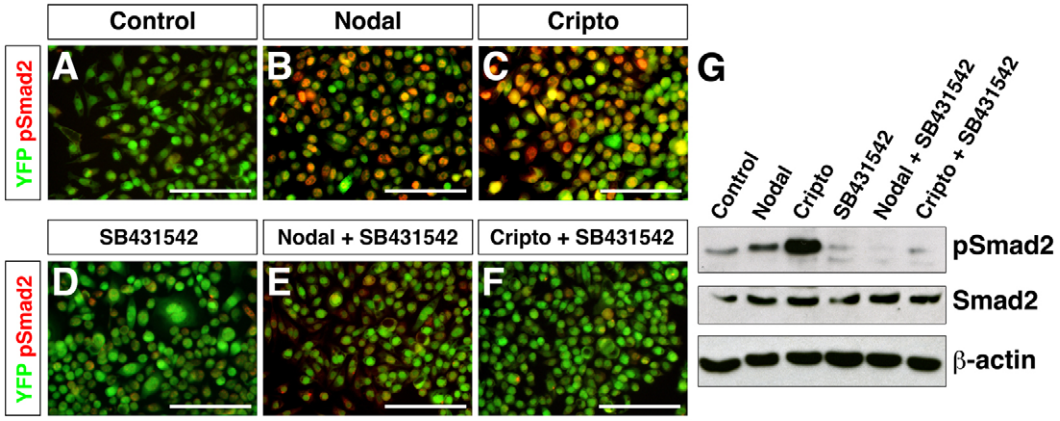


**Fig. 6. Nodal and Cripto induce Smad2 phosphorylation in XEN cells.** (**A-C**) Treatment of YFP-expressing mouse XEN cells with recombinant Nodal or Cripto for 1 hour results in upregulation of phosphorylated Smad2 (pSmad2). (**D-F**) Treatment with SB431542 blocks the upregulation of pSmad2 in response to Nodal or Cripto. (**G**) Western blot analysis of pSmad2, total Smad2, and beta-actin expression in XEN cells treated with Nodal, Cripto and/or SB431542 for 1 hour. Scale bars: 50 μm.

Although previous work has shown that Nodal signaling is required for DVE formation and translocation, the precise embryological origins and relationship of the DVE and AVE have been unclear. Previous studies have suggested that the expression patterns of *Lefty1* and *Cerl* at the late blastocyst stage correspond to an early specification of the DVE at peri-implantation stages (Takaoka et al., 2006; Torres-Padilla et al., 2007). Indeed, recent lineage-tracing studies indicate that the AVE has a separate origin from the DVE and is newly derived from the EmVE at 5.5 dpc (Takaoka et al., 2011). Such an independent origin of the AVE is consistent with the delayed or absent expression of some AVE markers in *Cripto* mutant embryos (Chu and Shen, 2010). In this regard, we note that our study has not addressed whether DVE (as opposed to AVE) might arise as a distinct response of XEN cells, or whether DVE heterogeneity might result from differential responses to independent Nodal and Cripto signaling pathways.

Interestingly, recent studies have described the isolation of XEN-like (XEN-P) cells from rat blastocysts (Debeb et al., 2009), which can contribute to both visceral and parietal endoderm as well as to trophoblast in chimeric rat embryos in the absence of prior Nodal treatment (Galat et al., 2009). However, these rat XEN-P cells display key differences to mouse XEN cells, as they are cultured in the presence of leukemia inhibitory factor (Lif) and express the pluripotency marker *Oct4* (Debeb et al., 2009). These findings suggest the existence of species-specific differences in XEN cell properties and/or possible differences in cell types that arose through isolation under distinct culture conditions. Indeed, recent gene expression profiling analyses have demonstrated considerable differences in gene expression between XEN cells and similar primitive endoderm-like lines derived from embryonal carcinoma cells (Brown et al., 2010). Consequently, it might be possible to derive a spectrum of XEN-like cell lines using distinct culture conditions.

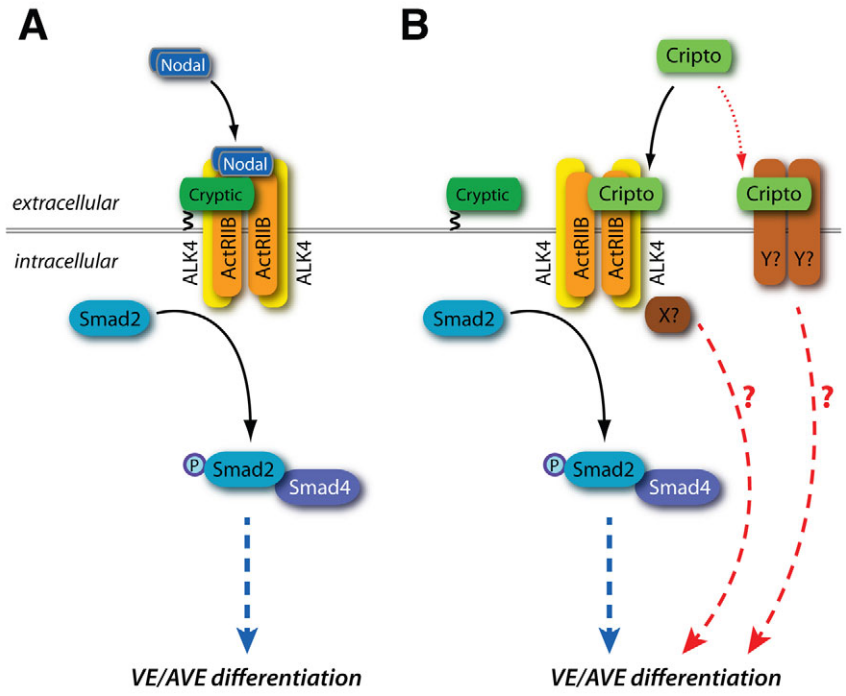


**Fig. 7. Model of the role of the Nodal and Cripto signaling pathways in mouse XEN cell differentiation.** (**A**) Nodal signaling through Alk4 is Cryptic dependent and leads to Smad2 phosphorylation. This canonical pathway eventually leads to visceral endoderm and AVE differentiation (blue dashed arrow). (**B**) In the absence of Nodal, Cripto can signal through Alk4 to promote Smad2 phosphorylation, which may lead to visceral endoderm and AVE differentiation; this Cripto activity could conceivably be mediated through Alk4 binding by an unknown TGFβ ligand that is distinct from Nodal. However, the ability of Cripto to promote visceral endoderm and AVE differentiation is at least partially independent of Alk4 kinase activity and Smad2 phosphorylation, as it is not blocked by SB431542. Thus, Cripto can also signal in a non-canonical pathway (red dashed lines), either through Alk4 in a kinase-independent manner through an unknown signal transducer 'X' or through an unknown cell-surface receptor 'Y' that can also mediate visceral endoderm and AVE differentiation. VE, visceral endoderm; AVE, anterior visceral endoderm.

Finally, recent work has shown that visceral endoderm cells can contribute to definitive endoderm in vivo (Kwon et al., 2008). Given the strong molecular similarity between the visceral and definitive endoderm, and the central role of Nodal signaling in definitive endoderm formation, our results raise the possibility that XEN, or XEN-like, cells might also be capable of contributing to definitive endoderm tissues.

**Acknowledgements**
We thank Janet Rossant for generously providing EYFP-expressing XEN cells, Vivienne Halili for assistance with microinjection, Po-Chien Chou for initial data on Smad2 phosphorylation, Parla Makinistoglu for assistance in generating XEN lines, and Gloria Kwon and Kat Hadjantonakis for advice on immunostaining. This work was supported by NIH grant HD42837 (M.M.S.). Deposited in PMC for release after 12 months.

**Competing interests statement**
The authors declare no competing financial interests.

**Supplementary material**
Supplementary material for this article is available at
http://dev.biologists.org/lookup/suppl/doi:10.1242/dev.065656/-/DC1

**References**
**Adkins, H. B., Bianco, C., Schiffer, S. G., Rayhorn, P., Zafari, M., Cheung, A. E., Orozco, O., Olson, D., De Luca, A., Chen, L. L. et al.** (2003). Antibody blockade of the Cripto CFC domain suppresses tumor cell growth in vivo. *J. Clin. Invest.* **112**, 575-587.
**Andersson, O., Reissmann, E., Jornvall, H. and Ibanez, C. F.** (2006). Synergistic interaction between Gdf1 and Nodal during anterior axis development. *Dev. Biol.* **293**, 370-381.
**Andersson, O., Bertolino, P. and Ibanez, C. F.** (2007). Distinct and cooperative roles of mammalian Vg1 homologs GDF1 and GDF3 during early embryonic development. *Dev. Biol.* **311**, 500-511.
**Andersson, O., Korach-Andre, M., Reissmann, E., Ibanez, C. F. and Bertolino, P.** (2008). Growth/differentiation factor 3 signals through ALK7 and regulates accumulation of adipose tissue and diet-induced obesity. *Proc. Natl. Acad. Sci. USA* **105**, 7252-7256.
**Arnold, S. J. and Robertson, E. J.** (2009). Making a commitment: cell lineage allocation and axis patterning in the early mouse embryo. *Nat. Rev. Mol. Cell Biol.* **10**, 91-103.
**Artus, J., Panthier, J. J. and Hadjantonakis, A. K.** (2010). A role for PDGF signaling in expansion of the extra-embryonic endoderm lineage of the mouse blastocyst. *Development* **137**, 3361-3372.
**Benjamini, Y. and Hochberg, Y.** (1995). Controlling the false discovery rate: a practical and powerful approach to multiple testing. *J. R. Stat. Soc. B* **57**, 289-300.
**Bianco, C., Adkins, H. B., Wechselberger, C., Seno, M., Normanno, N., De Luca, A., Sun, Y., Khan, N., Kenney, N., Ebert, A. et al.** (2002). Cripto-1 activates Nodal- and ALK4-dependent and -independent signaling pathways in mammary epithelial cells. *Mol. Cell. Biol.* **22**, 2586-2597.
**Bianco, C., Strizzi, L., Rehman, A., Normanno, N., Wechselberger, C., Sun, Y., Khan, N., Hirota, M., Adkins, H., Williams, K. et al.** (2003). A Nodal- and ALK4-independent signaling pathway activated by Cripto-1 through Glypican-1 and c-Src. *Cancer Res.* **63**, 1192-1197.
**Brennan, J., Lu, C. C., Norris, D. P., Rodriguez, T. A., Beddington, R. S. and Robertson, E. J.** (2001). Nodal signalling in the epiblast patterns the early mouse embryo. *Nature* **411**, 965-969.
**Brown, K., Legros, S., Artus, J., Doss, M. X., Khanin, R., Hadjantonakis, A. K. and Foley, A.** (2010). A comparative analysis of extra-embryonic endoderm cell lines. *PLoS ONE* **5**, e12016.
**Chen, C. and Shen, M. M.** (2004). Two modes by which Lefty proteins inhibit Nodal signaling. *Curr. Biol.* **14**, 618-624.
**Chen, C., Ware, S. M., Sato, A., Houston-Hawkins, D. E., Habas, R., Matzuk, M. M., Shen, M. M. and Brown, C. W.** (2006). The Vg1-related protein Gdf3 acts in a Nodal signaling pathway in the pre-gastrulation mouse embryo. *Development* **133**, 319-329.
**Chen, X., Rubock, M. J. and Whitman, M.** (1996). A transcriptional partner for MAD proteins in TGF-beta signalling. *Nature* **383**, 691-696.
**Chen, X., Weisberg, E., Fridmacher, V., Watanabe, M., Naco, G. and Whitman, M.** (1997). Smad4 and FAST-1 in the assembly of activin-responsive factor. *Nature* **389**, 85-89.
**Cheng, S. K., Olale, F., Bennett, J. T., Brivanlou, A. H. and Schier, A. F.** (2003). EGF-CFC proteins are essential coreceptors for the TGF-beta signals Vg1 and GDF1. *Genes Dev.* **17**, 31-36.
**Chu, J. and Shen, M. M.** (2010). Functional redundancy of EGF-CFC genes in epiblast and extraembryonic patterning during early mouse embryogenesis. *Dev. Biol.* **342**, 63-73.
**Chu, J., Ding, J., Jeays-Ward, K., Price, S. M., Placzek, M. and Shen, M. M.** (2005). Non-cell-autonomous role for Cripto in axial midline formation during vertebrate embryogenesis. *Development* **132**, 5539-5551.
**Debeb, B. G., Galat, V., Epple-Farmer, J., Iannaccone, S., Woodward, W. A., Bader, M., Iannaccone, P. and Binas, B.** (2009). Isolation of Oct4-expressing extraembryonic endoderm precursor cell lines. *PLoS ONE* **4**, e7216.
**Du, P., Kibbe, W. A. and Lin, S. M.** (2008). lumi: a pipeline for processing Illumina microarray. *Bioinformatics* **24**, 1547-1548.
**Ebert, A. D., Wechselberger, C., Frank, S., Wallace-Jones, B., Seno, M., Martinez-Lacaci, I., Bianco, C., De Santis, M., Weitzel, H. K. and Salomon, D. S.** (1999). Cripto-1 induces phosphatidylinositol 3′-kinase-dependent phosphorylation of AKT and glycogen synthase kinase 3β in human cervical carcinoma cells. *Cancer Res.* **59**, 4502-4505.
**Galat, V., Binas, B., Iannaccone, S., Postovit, L. M., Debeb, B. G. and Iannaccone, P.** (2009). Developmental potential of rat extraembryonic stem cells. *Stem Cells Dev.* **18**, 1309-1318.
**Gray, P. C., Harrison, C. A. and Vale, W.** (2003). Cripto forms a complex with activin and type II activin receptors and can block activin signaling. *Proc. Natl. Acad. Sci. USA* **100**, 5193-5198.
**Gray, P. C., Shani, G., Aung, K., Kelber, J. and Vale, W.** (2006). Cripto binds transforming growth factor beta (TGF-beta) and inhibits TGF-beta signaling. *Mol. Cell. Biol.* **26**, 9268-9278.
**Gritsman, K., Zhang, J., Cheng, S., Heckscher, E., Talbot, W. S. and Schier, A. F.** (1999). The EGF-CFC protein one-eyed pinhead is essential for Nodal signaling. *Cell* **97**, 121-132.
**Hadjantonakis, A. K., Gertsenstein, M., Ikawa, M., Okabe, M. and Nagy, A.** (1998). Generating green fluorescent mice by germline transmission of green fluorescent ES cells. *Mech. Dev.* **76**, 79-90.
**Inman, G. J., Nicolas, F. J., Callahan, J. F., Harling, J. D., Gaster, L. M., Reith, A. D., Laping, N. J. and Hill, C. S.** (2002). SB-431542 is a potent and specific inhibitor of transforming growth factor-beta superfamily type I activin receptor-like kinase (ALK) receptors ALK4, ALK5, and ALK7. *Mol. Pharmacol.* **62**, 65-74.
**Kelber, J. A., Shani, G., Booker, E. C., Vale, W. W. and Gray, P. C.** (2008). Cripto is a noncompetitive activin antagonist that forms analogous signaling complexes with activin and nodal. *J. Biol. Chem.* **283**, 4490-4500.
**Kumar, A., Novoselov, V., Celeste, A. J., Wolfman, N. M., ten Dijke, P. and Kuehn, M. R.** (2001). Nodal signaling uses activin and transforming growth factor-beta receptor-regulated Smads. *J. Biol. Chem.* **276**, 656-661.
**Kunath, T., Arnaud, D., Uy, G. D., Okamoto, I., Chureau, C., Yamanaka, Y., Heard, E., Gardner, R. L., Avner, P. and Rossant, J.** (2005). Imprinted X-inactivation in extra-embryonic endoderm cell lines from mouse blastocysts. *Development* **132**, 1649-1661.
**Kwon, G. S., Viotti, M. and Hadjantonakis, A. K.** (2008). The endoderm of the mouse embryo arises by dynamic widespread intercalation of embryonic and extraembryonic lineages. *Dev. Cell* **15**, 509-520.
**Lim, W. K., Lyashenko, E. and Califano, A.** (2009). Master regulators used as breast cancer metastasis classifier. *Pac. Symp. Biocomput.* **2009**, 504-515.
**Mesnard, D., Guzman-Ayala, M. and Constam, D. B.** (2006). Nodal specifies embryonic visceral endoderm and sustains pluripotent cells in the epiblast before overt axial patterning. *Development* **133**, 2497-2505.
**Migeotte, I., Omelchenko, T., Hall, A. and Anderson, K. V.** (2010). Rac1-dependent collective cell migration is required for specification of the anterior-posterior body axis of the mouse. *PLoS Biol.* **8**, e1000442.
**Minchiotti, G., Parisi, S., Liguori, G., Signore, M., Lania, G., Adamson, E. D., Lago, C. T. and Persico, M. G.** (2000). Membrane-anchorage of Cripto protein by glycosylphosphatidylinositol and its distribution during early mouse development. *Mech. Dev.* **90**, 133-142.
**Nagy, A., Gertsenstein, M., Vintersten, K. and Behringer, R.** (2003). *Manipulating the Mouse Embryo: A Laboratory Manual*. Cold Spring Harbor, NY: Cold Spring Harbor Laboratory Press.
**Norris, D. P., Brennan, J., Bikoff, E. K. and Robertson, E. J.** (2002). The FoxH1-dependent autoregulatory enhancer controls the level of Nodal signals in the mouse embryo. *Development* **129**, 3455-3468.
**Ramakers, C., Ruijter, J. M., Deprez, R. H. and Moorman, A. F.** (2003). Assumption-free analysis of quantitative real-time polymerase chain reaction (PCR) data. *Neurosci. Lett.* **339**, 62-66.
**Reissmann, E., Jornvall, H., Blokzijl, A., Andersson, O., Chang, C., Minchiotti, G., Persico, M. G., Ibanez, C. F. and Brivanlou, A. H.** (2001). The orphan receptor ALK7 and the Activin receptor ALK4 mediate signaling by Nodal proteins during vertebrate development. *Genes Dev.* **15**, 2010-2022.
**Rivera-Perez, J. A., Mager, J. and Magnuson, T.** (2003). Dynamic morphogenetic events characterize the mouse visceral endoderm. *Dev. Biol.* **261**, 470-487.
**Rossant, J. and Tam, P. P.** (2009). Blastocyst lineage formation, early embryonic asymmetries and axis patterning in the mouse. *Development* **136**, 701-713.
**Schier, A. F.** (2009). Nodal morphogens. *Cold Spring Harb. Perspect. Biol.* **1**, a003459.
**Shani, G., Fischer, W. H., Justice, N. J., Kelber, J. A., Vale, W. and Gray, P. C.** (2008). GRP78 and Cripto form a complex at the cell surface and collaborate to

inhibit transforming growth factor beta signaling and enhance cell growth. *Mol. Cell. Biol.* **28**, 666-677.
**Shen, M. M.** (2007). Nodal signaling: developmental roles and regulation. *Development* **134**, 1023-1034.
**Smyth, G. K.** (2004). Linear models and empirical bayes methods for assessing differential expression in microarray experiments. *Stat. Appl. Genet. Mol. Biol.* **3**, Article 3.
**Srinivas, S., Rodriguez, T., Clements, M., Smith, J. C. and Beddington, R. S.** (2004). Active cell migration drives the unilateral movements of the anterior visceral endoderm. *Development* **131**, 1157-1164.
**Stuckey, D. W., Clements, M., Di-Gregorio, A., Senner, C. E., Le Tissier, P., Srinivas, S. and Rodriguez, T. A.** (2011). Coordination of cell proliferation and anterior-posterior axis establishment in the mouse embryo. *Development* **138**, 1521-1530.
**Subramanian, A., Tamayo, P., Mootha, V. K., Mukherjee, S., Ebert, B. L., Gillette, M. A., Paulovich, A., Pomeroy, S. L., Golub, T. R., Lander, E. S. et al.** (2005). Gene set enrichment analysis: a knowledge-based approach for interpreting genome-wide expression profiles. *Proc. Natl. Acad. Sci. USA* **102**, 15545-15550.
**Takaoka, K., Yamamoto, M., Shiratori, H., Meno, C., Rossant, J., Saijoh, Y. and Hamada, H.** (2006). The mouse embryo autonomously acquires anterior-posterior polarity at implantation. *Dev. Cell* **10**, 451-459.
**Takaoka, K., Yamamoto, M. and Hamada, H.** (2011). Origin and role of distal visceral endoderm, a group of cells that determines anterior-posterior polarity of the mouse embryo. *Nat. Cell Biol*. **13**, 743-752.
**Tanaka, C., Sakuma, R., Nakamura, T., Hamada, H. and Saijoh, Y.** (2007). Long-range action of Nodal requires interaction with GDF1. *Genes Dev.* **21**, 3272-3282.
**Thomas, P. Q., Brown, A. and Beddington, R. S. P.** (1998). *Hex*: a homeobox gene revealing peri-implantation asymmetry in the mouse embryo and an early transient marker of endothelial cell precursors. *Development* **125**, 85-94.
**Torres-Padilla, M. E., Richardson, L., Kolasinska, P., Meilhac, S. M., Luetke-Eversloh, M. V. and Zernicka-Goetz, M.** (2007). The anterior visceral endoderm of the mouse embryo is established from both preimplantation precursor cells and by de novo gene expression after implantation. *Dev. Biol.* **309**, 97-112.
**Trichas, G., Joyce, B., Crompton, L. A., Wilkins, V., Clements, M., Tada, M., Rodriguez, T. A. and Srinivas, S.** (2011). Nodal dependent differential localisation of dishevelled-2 demarcates regions of differing cell behaviour in the visceral endoderm. *PLoS Biol.* **9**, e1001019.
**Vallier, L., Alexander, M. and Pedersen, R. A.** (2005). Activin/Nodal and FGF pathways cooperate to maintain pluripotency of human embryonic stem cells. *J. Cell Sci.* **118**, 4495-4509.
**Watanabe, K., Nagaoka, T., Lee, J. M., Bianco, C., Gonzales, M., Castro, N. P., Rangel, M. C., Sakamoto, K., Sun, Y., Callahan, R. et al.** (2009). Enhancement of Notch receptor maturation and signaling sensitivity by Cripto-1. *J. Cell Biol.* **187**, 343-353.
**Yan, Y.-T., Gritsman, K., Ding, J., Burdine, R. D., Corrales, J. D., Price, S. M., Talbot, W. S., Schier, A. F. and Shen, M. M.** (1999). Conserved requirement for *EGF-CFC* genes in vertebrate left-right axis formation. *Genes Dev.* **13**, 2527-2537.
**Yan, Y. T., Liu, J. J., Luo, Y., E, C., Haltiwanger, R. S., Abate-Shen, C. and Shen, M. M.** (2002). Dual roles of Cripto as a ligand and coreceptor in the Nodal signaling pathway. *Mol. Cell. Biol.* **22**, 4439-4449.
**Yeo, C. and Whitman, M.** (2001). Nodal signals to Smads through Cripto-dependent and Cripto-independent mechanisms. *Mol. Cell* **7**, 949-957.
**Zernicka-Goetz, M., Morris, S. A. and Bruce, A. W.** (2009). Making a firm decision: multifaceted regulation of cell fate in the early mouse embryo. *Nat. Rev. Genet.* **10**, 467-477.

**Table S1. Primers (5′ to 3′) used for PCR analyses**

| Gene | Forward primer | Reverse primer |
|---|---|---|
| *ActRII* | GTCACACAGCCTACGTCGAA | TTGAGTTGGAACGAGCACAG |
| *ActRIIb* | ATGTGCCGTGGTGTCGTGGT | GACCTCCTGATCAGGGATAC |
| *Afp** | GCCCAGACATACGAAGAAAACA | TCTCTTTGTCTGGAAGCATTCCT |
| *Alk4* | GTGGTGACGTGGCTGTGAAA | TTTGGAGCAATGTCTATGGT |
| *Alk5* | GTCCGCAGCTCCTCATCGT | GACAGTGCGGTTATGGCAGAT |
| *Alk7* | TGGGGGACGAAATCATCAAG | GCGCACCTGCACCCCTCCAA |
| *Cerl* | TATGTGATGCCCCGACTGTA | GGGCACAGTCCTGCAGGTCT |
| *Cerl** | AAGTGGAGAGATCACCTCTA | GACACTCTTCGACTTGCATC |
| *Cripto* | ATGGACGCAACTGTGAACATGATGTTCGCA | CTTTGAGGTCCTGGTCCATCACGTGACCAT |
| *Cryptic* | CACCAACCCAGGGTATCAGTT | AGAGTTCTGTCCAGTGTCGTC |
| *Foxa2* | CCCTACGCCAACATGAACTCG | GTTCTGCCGGTAGAAAGGGA |
| *Foxh1* F | ATCCGTCAGGTCCAGGCAGTG | CTTGGCGAAAGCTCTGTG |
| *Gata6* | ACCTTATGGCGTAGAAATGCTGAGGGTG | CTGAATACTTGAGGTCACTGTTCTCGGG |
| *Gata6** | CGGGCGCAGGCAGTGAGT | CCAAGCCGCCGTGATGAAGG |
| *Gdf1* F | GTTGCGGCTGGAGGCTGAGAG | CCCACTGGACCAACTTCTACC |
| *Gdf3* F | GTTCCAACCTGTGCCTCGCGTCTT | AGCGAGGCAATGGAGAGAGCGGAGCAG |
| *hHex* | GTTCTCCAACGACCAGACCG | GGAGGGTGAACACTGCGAAC |
| *Hnf4a** | ACACGTCCCCATCTGAAGGTG | CTTCCTTCTTCATGCCAGCCC |
| *Lefty1* | AACCTTCGAGAGGTGGCAGG | GCCTTCCAGCCGCACTCGTG |
| *Nodal* F | AAGACCAAGCCACTGAGCAT | GCCTTTGCACACAATTTCAA |
| *Sox2* F | GGTTACCTCTTCCTCCCACTCCAG | TCACATGTGCGACAGGGGCAG |

*Primers for real-time PCR.

**Table S5. False discovery rate analysis**

| | Nodal | Cripto | Control |
|---|---|---|---|
| Nodal | 463±361 | 573±295 | 1648±820 |
| Cripto | | 506±375 | 2627±512 |

To estimate the rate of false discoveries, we computed the number of differentially expressed genes when comparing different replicates of Cripto treatment to each other, and different replicates of Nodal treatment to each other. Since we performed five replicates per treatment, we computed the number of differentially expressed genes from the 15 possible combinations of the five replicates taken by pairs. These results constitute a measure of the false discoveries. The table shows the mean ± s.d. for the number of differentially expressed genes at $P<0.01$ for 15 permutations of Nodal versus Nodal, Cripto versus Cripto, Nodal versus Cripto, Cripto versus control samples and Nodal versus control samples. The number of differentially expressed genes between Cripto and Nodal was not different as the Nodal versus Nodal ($P=0.36$) and Cripto versus Cripto ($P=0.59$). However, the number of genes responding to Nodal treatment was higher than Nodal versus Nodal comparison ($P<5.7E–5$), and the number of genes responding to Cripto treatment was higher than Cripto versus Cripto comparison ($P<1E–12$).